In Situ XPS Analysis of Tribo-chemical Behavior in Titanium Alloy Exposed to Fretting Wear Under the Vacuum Environments

Long, Jianjun; Wei, Xuejiao; Dong, Yiting; Cheng, Xixi; Li, Hao; Xu, Xiaojun; Zhu, Minhao

DOI
10.1007/s11249-024-01842-8

Publication date
2024

Document Version
Final published version

Published in
Tribology Letters

Tribology Letters (2024) 72:43
https://doi.org/10.1007/s11249-024-01842-8

ORIGINAL PAPER

In Situ XPS Analysis of Tribo-chemical Behavior in Titanium Alloy Exposed to Fretting Wear Under the Vacuum Environments

Jianjun Long[1] · Xuejiao Wei[1] · Yiting Dong[1] · Xixi Cheng[1] · Hao Li[1] · Xiaojun Xu[1,2] · Minhao Zhu[1]

Received: 2 September 2023 / Accepted: 20 February 2024

Abstract
A systematic experimental investigation concerning the fretting-induced tribo-chemical state and its effect on the fretting wear behavior of titanium alloys under the vacuum atmospheres (4×10^{-3} Pa and 4×10^{-1} Pa) in different fretting regimes is reported. An in situ XPS analysis tester was developed to capture the real tribo-chemical state of worn surface for all test conditions. Results show that samples subjected to different vacuum atmospheres have varied tribo-chemical states depending on the fretting regime, which play significantly different roles in determining the associated damage mechanisms and the resulting fretting wear resistance. Under both vacuum atmospheres, in the partial slip regime (PSR) the worn scars were mainly covered by TiO_2, showing comparable levels of very slight damage, while in the mixed fretting regime (MFR), the tribo-layer is still mainly consisted of TiO_2, but with an evident peak of Ti metal for the high vacuum degree (4×10^{-3} Pa) in MFR, showing a mild damage. In contrast, in the gross slip regime (GSR), Ti metal was prone to be oxidized to Ti_2O_3 and TiO on the worn scar, especially for the low vacuum degree (4×10^{-1} Pa) having a highest content of Ti_2O_3. It might be inferred that the tribo-layer containing more Ti_2O_3 formed during fretting wear process is susceptible to be broken, hence showing a highest fretting wear volume in GSR for the low vacuum degree. The results suggest that for the vacuum environments, the Ti6Al4V may be more suitable to be used under the high vacuum atmosphere.

Keywords Titanium alloy · In situ XPS · Vacuum atmosphere · Fretting wear · Tribo-chemical state

1 Introduction

Tribo-chemical reaction is a common tribological behavior invariably observed in tight fit assemblies during fretting wear process for industrial applications, such as aerospace engineering, naval craft, mineral processing, and nuclear engineering [1–3]. Titanium alloys due to their great combinations of the low density, high specific strength, excellent corrosion resistance and biocompatibility, have been often used in such industrial applications including those where the wear plays a key role, i.e., plunger, gear, bolts, the screws, nuts and rivets [1, 4]. With the development and the high demand on the industrial applications orienting towards the hash working conditions, such mechanical systems and structural components of titanium alloys were required to be used in various working atmospheres including the non-air atmosphere. For instance, the working environments of the aircraft and spacecraft will range from the air atmosphere to the space environment and will experience different vacuum degree atmospheres, which will hence lead to varied tribo-chemical reactions and then form different tribo-chemical products on the contact interface [5, 6]. Many studies [7–9] have revealed that the resulting tribo-chemical products during wear process play a significant influence on the wear behavior depending on the working environments. Hence, it is of great importance to probe the tribo-chemical state and study its role in determining the associated wear behavior.

There have been many works conducted to study the wear behavior of titanium alloys and received increasing attentions on the wear behaviors under the different test atmospheres. Nevertheless, the works to study wear behavior of titanium alloys are mostly conducted in the air atmosphere

✉ Xiaojun Xu
xiaojunxu0617@126.com; xiaojunxu@swjtu.edu.cn

[1] Key Laboratory of Advanced Technologies of Materials (Ministry of Education), School of Materials Science and Engineering, Southwest Jiaotong University, Chengdu 610031, China

[2] Novel Aerospace Materials Group, Faculty of Aerospace Engineering, Delft University of Technology, 2629HS Delft, The Netherlands

Published online: 22 March 2024

with the respect to the multi-aspect, such as the sliding speed and/or loading conditions [10–12], the temperature [13, 14], tribo-oxides layer [12, 15–17], which can be concluded that the wear mechanisms are dependent on the sliding speeds and/or loading conditions, and a compacted tribo-oxides layer can provide a protection against wear and then improve the wear resistance. In contrast, there are some researches on the wear behavior of titanium alloys under the non-air atmosphere. Mercer et al. [18] compared the wear resistance of Ti–6Al–4V alloy under dry inert gas (argon and nitrogen) and dry air conditions, and found that the abrasive wear rate in inert gas atmosphere was significantly lower than that in air atmosphere, which was considered to be due to the possibility that abrasive wear in inert gas environment may lead to a change in the contact surface products of titanium alloys and then improved the surface ductility. Liu et al. [19] studied the wear behavior of Ti–6Al–4V in vacuum and in air atmosphere, and the results demonstrated that the wear rate in vacuum was substantially lower than that in air under all sliding speeds and loads, which suggested that it could be due to the formation of nanostructure in subsurface and a large number of dislocations under vacuum condition due to the adhesion. In another studies related to the comparison in wear resistance of titanium alloys in air and vacuum conditions, some investigations [6, 19, 20] reported that the wear rate of titanium alloys in vacuum and in air was strongly dependent on the sliding rate, and further pointed out that there is a critical sliding rate within which the wear rate in vacuum was lower than that in air, but beyond which the wear rate in vacuum was higher than that in air due to the oxide layer produced in air hence lowering the wear rates [21]. Moreover, Zhong et al. [22] concentrated on vacuum atmosphere to study the tribological properties of titanium alloys, and the results showed that the sliding wear volumes increased monotonically with the sliding velocities. The observations demonstrated that at the lower sliding velocity the main wear mechanism was abrasive wear, while at the highest sliding velocity the dominant wear mechanisms was the severe delamination and plastic deformation. In addition, Yazdanian et al. [23] studied the sliding wear behavior of thermally oxidized Ti–6Al–4V under the vacuum condition, and the results showed that the TiO_2 layer formed in the surface prevent surface plastic deformation to reduce wear rate under the vacuum sliding. Notwithstanding these studies make a significant progress in understanding of wear behavior of titanium alloys, till now the works on the wear behavior of titanium alloys either focused on the sliding wear or the air atmospheres. Systematic investigations into the fretting-induced tribo-chemical behavior of titanium alloys under the vacuum atmosphere are still lacking. Although a few researches concerning the fretting wear of titanium alloys have been conducted and demonstrated that the formation of TiO_x can improve the fretting wear resistance [8, 24], they are mainly limited in the case of the air atmospheres. Therefore, the response of tribo-chemical products on fretting wear under vacuum atmosphere is still not yet clear.

The aim of the present work is to clarify the real tribo-chemical state of worn surface in the vacuum atmospheres during fretting wear process by using an in situ XPS analysis tester and study its effect on the fretting wear behavior. The in situ XPS analysis tester was developed by a self-designed high precision fretting wear tester integrated with an X-ray photoelectron spectroscopy (XPS) equipment. In the current paper, a Ti6Al4V titanium alloy was selected and different vacuum degrees atmospheres were chosen. The tribo-chemical products of Ti6Al4V titanium alloy in the different fretting regimes are investigated. The worn scar and the associated damage mechanisms upon different test conditions are analyzed, and the correlation of tribo-chemical state with the resulting damage mechanism and the fretting wear resistance are discussed. In addition, the fretting wear resistance of Ti6Al4V titanium alloy under the vacuum atmospheres was compared to that under the air atmosphere.

2 Experimental Procedures

2.1 Materials and Sample Preparation

In the present study, a commercial Ti6Al4V titanium alloy plate obtained by annealing at 750 °C for 3 h followed by air cooling was chosen. It has a Vickers's hardness of 320. Prior to the fretting wear tests, samples were mounted and polished by automatic polishing machine (AutoMet 250), obtaining a final surface roughness (Ra) of 0.03 μm. The specimens for fretting wear tests were prepared with the size of 15 mm × 10 mm × 3 mm. GCr15 steel with the diameter of 10 mm, the roughness of 0.05 μm and Vickers's hardness of 690 was used as counter-body in the current study. All samples were ultrasonically cleaned for 10 min with alcohol to guarantee the removal of pollution on the surface before fretting wear tests, and then were immersed inside the alcohol for the protection from exposure to the atmosphere.

2.2 Fretting Wear Tests

In order to realize the in situ observation on the tribo-chemical state of worn surface of Ti6Al4V titanium alloy, the fretting wear tests were performed on a self-designed high precision fretting wear testing machine assembled with an X-ray photoelectron spectroscopy (XPS) equipment. This method can capture the real tribo-chemical products of worn surface via the process of directly transferring the sample after fretting wear in a specific atmosphere into the XPS chamber without the exposure to the air environment. The

in situ XPS test is different from the conventional XPS tests where the tested samples after wear test would be exposed inevitably to the air atmosphere when transferred to XPS chamber and hence the resulting worn scar can be oxidized under the air atmosphere during transfer process. A detailed schematic drawing of the fretting wear test equipped with an in situ XPS analysis device is shown in Fig. 1. In the experimental setup the fretting wear test device was connected with XPS device via a corrugated pipe involved a gate valve inside. Figure 1b gives the schematic drawing of the fretting wear test part, in which the specimen placed on the table was driven by a piezoelectric ceramic actuator. A grating displacement sensor was located on the lateral side of sample holder on table as shown in Fig. 1b. The grating ruler of the displacement sensor was stick on the lateral side of sample holder. As the fretting occurred due to the actuator, the sample fixed on the sample holder would have the displacement variation, and meanwhile the read head of the displacement sensor read and record the displacement difference, which can give a real-time feedback of displacement to actuator, so as to approach a high precision of about ± 0.1 μm for the displacement control, as described in Ref. [25].

The fretting wear tests were conducted under the different vacuum degrees of atmospheres. After the completion of fretting wear test, the magnetic control rod marked with "1" in Fig. 1a will be pushed into the fretting wear test chamber to catch the sample holder (seen in Fig. 1c), while the loading cell was unloaded and the fastening screw to tighten the sample was released by rotating the left level device. The next step is to open the gated valve between the wear test chamber and XPS sample chamber, and then transfer the sample by using the magnetic control rod to the sample shelf (seen in Fig. 1c) with which the sample can then be delivered to the XPS sample chamber as marked with "5" in Fig. 1a. Finally, after the gated valve was closed and the XPS sample chamber was evacuated to 1×10^{-5} Pa equivalent to that of XPS working chamber (as marked with "6" in Fig. 1a), the sample was directly moved into the XPS working chamber for tribo-chemistry analysis. The whole experimental process took place in a closed environment without exposure to air, as stated in previous study [26]. In addition, it is worth pointing out that in the current experimental setups, the counter body (GCr15) was fixed on the clamping device, which cannot be disassembled from the clamping device without opening the chamber door after wear tests. Therefore, the real tribo-chemical state of counter-body (GCr15) cannot be studied in the current study.

The fretting wear tests in the current work were conducted under the normal load of 20N with the various displacement amplitudes, i.e., 1 μm, 5 μm, 10 μm, 20 μm, 30 μm, 40 μm. Here, the displacement amplitude was defined the maximum value of relative displacement between sample and counter-body with respect to the starting point of fretting wear. Based on the loading condition and the material parameters, the elastic Hertz contact radius has been calculated, and it is much larger than all

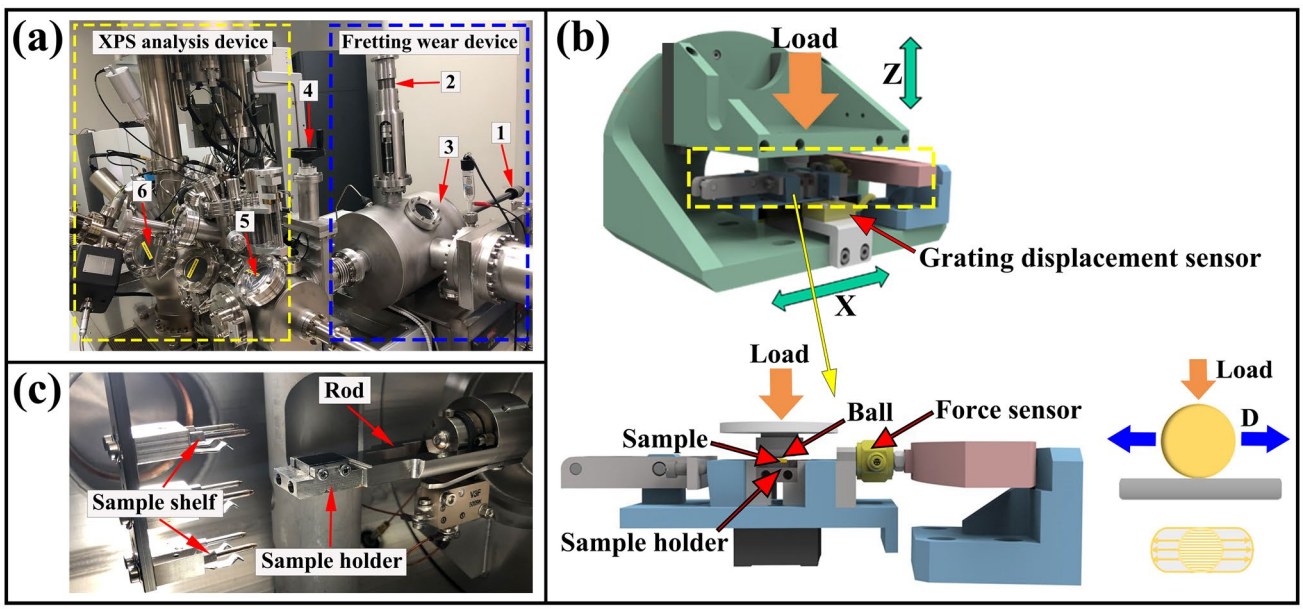

Fig. 1 A schematic drawing of the fretting wear tester integrated with an XPS analysis device. **a** External view: (1) Magnetic control rod for delivering the sample; (2) Loading device; (3) The chamber of friction wear test; (4) Gate valve; (5) XPS delivering sample chamber; (6) XPS working chamber; **b** A schematic drawing of the fretting wear test; **c** Internal view of delivering sample from wear test chamber to XPS chamber

displacement amplitudes chosen, which make sure that the wear process is belonging to the fretting wear. Two different degrees of vacuum atmospheres were adopted, i.e., 4×10^{-3} Pa, 4×10^{-1} Pa. Each test was repeated 3 times to make sure that reproducibility was observed and reported. The detailed test parameters selected are list in Table 1.

2.3 Worn Scar Observation

The tribo-chemical state on the worn scar was analyzed by the X-ray photoelectron spectroscopy (XPS, ESCALAB 250Xi, Thermo). After finished the analysis of XPS, the morphologies of the worn scars were observed by a scanning electron microscopy (SEM, JSM-6610, JOEL). The wear loss and the profiles of worn scar were quantified by a white light interferometer (WLI, GTK-16-0295, Bruker).

Table 1 The test parameters of fretting wear test

Test parameters	
Normal load	20 N
Displacement amplitude	1 μm, 5 μm, 10 μm, 20 μm, 30 μm, 40 μm
Frequency	2 Hz
Cycles numbers	1×10^4
Atmosphere parameter	4×10^{-3} Pa, 4×10^{-1} Pa

3 Results and Discussions

3.1 Fretting Regimes

The evolutions of fretting hysteresis loops consisted of frictional force (F_t) versus displacement amplitude (D) as functions of cycles are often employed to distinguish the fretting regimes of worn surface. According to the work of Zhou et al. [27, 28], three fretting regimes, i.e., partial slip regime (PSR), mixed fretting regime (MFR) and gross slip regime (GSR), can be well examined on the basis of the shape of F_t–D–N curves. Figure 2 presents one cycle of the F_t–D–N curves at the steady stage under the imposed normal load 20 N with the different displacements, with which three typical fretting regimes can be well observed based on the shape of the F_t–D curves under the 4×10^{-3} Pa, 4×10^{-1} Pa, respectively. In the case of $P=4\times10^{-1}$ Pa, at a low displacement amplitude around (less than) 1 μm, the displacement is mainly accommodated by elastic deformation and hence the F_t–D curve presents a nearly line shape as shown in Fig. 2a, which reveals that the fretting process runs in the partial slip regime (PSR) under such working conditions. As the displacement amplitude increases to a higher value ($D>10$ μm), there is evident relative displacement motion along with serious plastic deformation and hence all F_t–D curves are open and display a quasi-rectangular shape as shown in Fig. 2d–f, suggesting a gross slip regime (GSR) [28]. Nonetheless, they indeed show somewhat difference in the friction force (i.e., friction coefficient), which should relate to the state of contact interface depending on the vacuum degree, such as the tribo-oxides, the formation and removal of debris. While for an intermediate displacement amplitude such as 5 μm and 10 μm, the F_t–D curve presents an elliptical shape of loop as demonstrated in Fig. 2b, c,

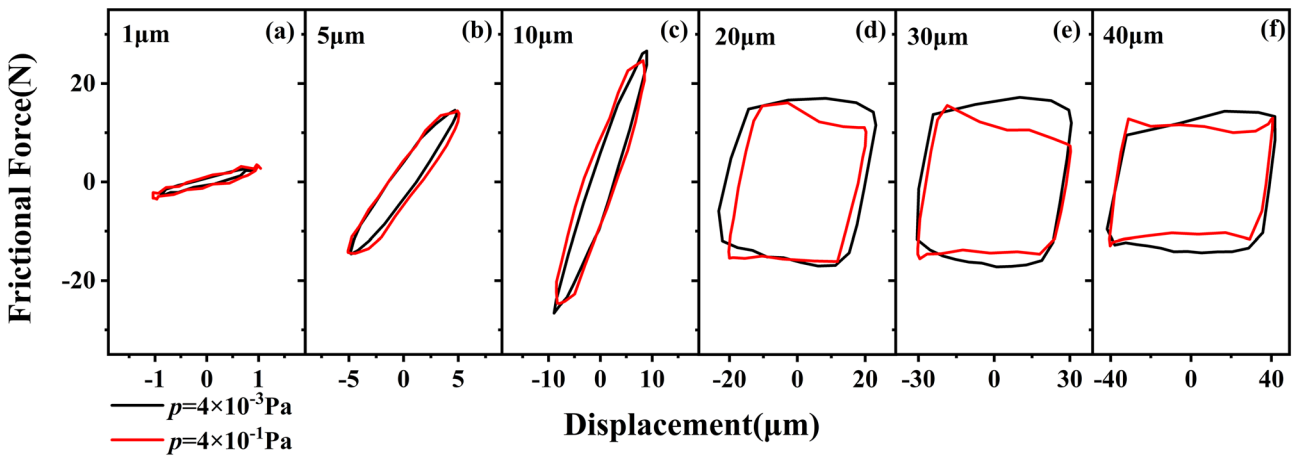

Fig. 2 The evolutions of fretting hysteresis loops under the vacuum atmospheres ($F_n=20$ N, $N=10^4$)

Table 2 The value of energy ratio A

Displacement amplitude (μm)	A (energy ratio) for 4×10^{-1} Pa	A (energy ratio) for 4×10^{-3} Pa
1	0.19	0.17
5	0.20	0.18
10	0.20	0.17
20	0.73	0.71
30	0.75	0.75
40	0.77	0.77

referring to MFR where the contact interfaces were mainly coordinated by the elastoplastic deformation [29]. While for the higher vacuum degree of 4×10^{-3} Pa, it presents largely similar fretting loops evolutions to those under 4×10^{-1} Pa. In order to make sure the accuracy in distinguishing the fretting regimes by the *Ft–D* curve, the energy ratio A as proposed by Fouvry et al. [30] was also calculated as shown in Table 2. Based on the Fouvry's work, the energy ration A of 0.2 can be considered as the estimated boundary of the partial slip state and the gross slip state distinguished. It can be seen that the criteria to distinguish the fretting wear region by energy ratio A is largely consistent with that by the shape of *Ft–D* curve in the current investigation.

Moreover, compared to the previous investigation on the fretting regimes for the air atmosphere [27], the main difference is that the region of MFR (5 μm ≤ D < 20 μm) under the vacuum atmosphere is broader than that under air environment, which could be attributed to the possibility that under the vacuum environment the contact interface is more susceptible to stick slip and hence lead to hardly slip. Under the vacuum, the original pre-oxidized film on the Ti metal can be easily ruptured and removed after some fretting wear cycles, and then a fresh Ti metal would be exposed. Compared to the air atmosphere, the exposed fresh Ti metal was more difficult to be re-oxidized under the vacuum atmosphere in the subsequent fretting wear process. As a result, the contact interface between fresh Ti metal and counter-body is easy to form welding and hence cause adhesion effect, hence hind the slip and then broaden the region of MFR [31].

3.2 Tribo-chemical States of Worn Surface in Different Fretting Regimes

The in situ XPS analysis tests presented here can realize the process of transferring the sample after fretting wear in a specific environment directly into the XPS chamber without exposure to the air environment, and can well probe a real tribo-chemical state. In order to benchmark the conventional XPS analysis method, the Fig. 3 gives the difference

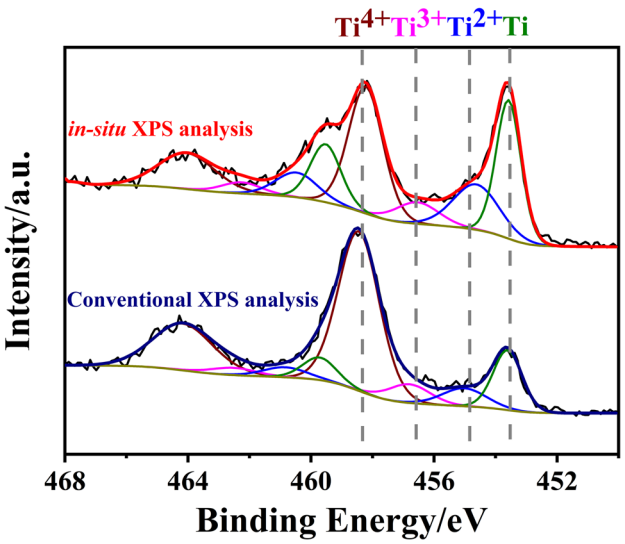

Fig. 3 Ti 2p spectra on the worn scars in the vacuum atmospheres for the in situ and conventional XPS analysis (F_n = 20 N, D = 30 μm)

in chemical state of worn surface between the conventional XPS analysis and in situ XPS analysis with regard to the Ti 2p spectra under the vacuum atmosphere of 4×10^{-3} Pa. It should be noticed here that in XPS analysis, all spectra were calibrated by the C 1s peak with the standard binding energy of 284.8 eV. As can be seen in Fig. 3, the spectra of Ti 2p are all consisted of four components identified as Ti^{4+} $2p_{3/2}$ (458.5 eV), Ti^{3+} $2p_{3/2}$ (456.9 eV), Ti^{2+} $2p_{3/2}$ (455.0 eV) and Ti $2p_{3/2}$ (453.9 eV), which correspond to TiO_2, Ti_2O_3, TiO and Ti, respectively. Nonetheless, there is a significant difference in XPS results between both. Compared with in situ XPS analysis results, there is a higher percentage of TiO_2 content but much lower percentage of Ti metal in the conventional XPS analysis, which indicates the occurrence of continuous oxidation of Ti metal on the worn surface as exposed to the air atmosphere during the process of transferring the sample to the XPS chamber. It further indicates that the conventional XPS analysis cannot properly probe the real tribo-chemical state produced during fretting wear process under the non-air atmosphere.

Considering that the Ti spectra are expected to better represent the chemical state of not only the Ti itself but also the corresponding O element, in the current study the Ti spectra were selected for the analysis of tribo-chemical state of the worn surface. Figures 4, 5 and 6 present in situ XPS analysis results on the chemical state of worn surface produced in different fretting running regimes, i.e., PSR (D = 1 μm, seen in Fig. 4), MFR (D = 5 μm, seen in Fig. 5) and GSR (D = 30 μm, seen in Fig. 6) with the normal load of 20 N under the 4×10^{-3} Pa, and 4×10^{-1} Pa, respectively. The resulting content percentage of oxides on the worn scar for all test conditions are list in Table 3.

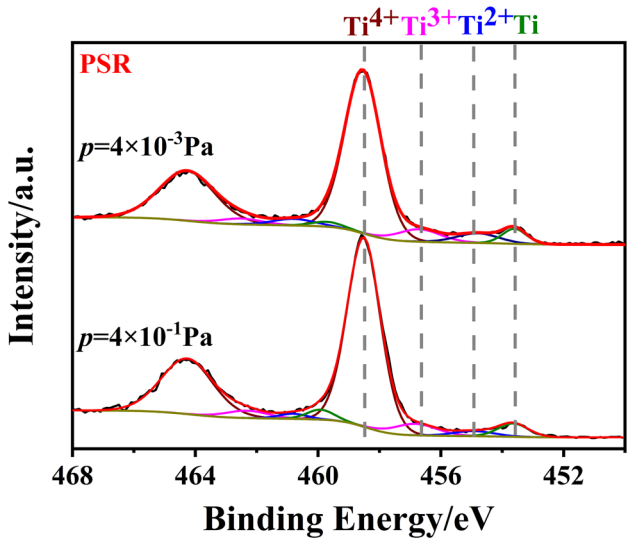

Fig. 4 XPS spectra of Ti 2p on the worn scars in PSR ($D = 1$ μm)

In the case of PSR ($D = 1$ μm), as can be seen in Fig. 4, regardless of the test atmospheres the main peaks of Ti 2p are all Ti^{4+} spectra at 458.5 eV corresponding to the TiO_2, along with very weak peaks of Ti, Ti^{2+} (TiO) and Ti^{3+} (Ti_2O_3). Based on the previous study on the XPS analysis of the initial surface of polished samples [27], the dominant TiO_2 could be mainly originated from the initial surface of polished samples. It implies that the contact interface was suffered from very slight damage, which is well consistent with the nature of partial slip regime. With the increase of displacement amplitude up to 5 μm, the fretting regime enters the MFR. On the basis of the XPS survey spectra in MFR as seen in Fig. 5a, it can be seen that although the counter-body is GCr15 steel, no Fe peak can be found on the worn surface, i.e., no material of the counter-body has transferred, which is also applied to the case of PSR. The cause could be attributed to the marginal displacement movement in MFR and PSR. Therefore, only the XPS results of Ti 2p were given for the MFR. As seen in Fig. 5b, the XPS spectra seems to be some different from that in PSR. Except for the main peaks of Ti 2p spectra at 458.5 eV corresponding to the TiO_2, there is an evident peak of Ti metal at 453.9 eV. As shown in Table 3, the percentage of Ti metal content for the 4×10^{-3} Pa and 4×10^{-1} Pa are 13%, 7%, respectively. Compared to the PSR, the clear evidence of Ti metal peak suggests that there is more exposure of Ti matrix in MFR, especially for 4×10^{-3} Pa vacuum conditions, which could be relevant to the oxygen-poor atmosphere. Nevertheless, for all testing atmospheres the peaks of Ti 2p spectra (TiO_2) are still dominant, i.e.,72% TiO_2 for 4×10^{-3} Pa, and 81% TiO_2 for 4×10^{-1} Pa (seen in Table 3).

In the case of GSR ($D = 30$ μm), the XPS survey spectra is similar to that in MFR (seen in Fig. 6a), i.e., no Fe 2p peak but Ti 2p peak can be found, which also indicates no counter-body material transfer occurred under the vacuum atmosphere. As observed, under the vacuum conditions (4×10^{-3} Pa and 4×10^{-1} Pa), the XPS result in GSR is quite different from MFR and PSR. Besides the peak of Ti^{+4} (TiO_2), there are significantly evident peaks of Ti metal, Ti^{2+} (TiO) and Ti^{3+} (Ti_2O_3) peak in the GSR, which implies that Ti metal was prone to be oxidized to Ti^{3+} (Ti_2O_3) and Ti^{2+} (TiO) under the vacuum atmosphere in GSR. As listed in Table 3, the Ti 2p for 4×10^{-1} Pa atmosphere are composed of 40%TiO_2, 18%Ti_2O_3, 21%TiO, and 21%Ti, while for 4×10^{-3} Pa the Ti 2p are consisted of 40%TiO_2, 8%Ti_2O_3, 20%TiO, and 32%Ti. It demonstrates that under the low

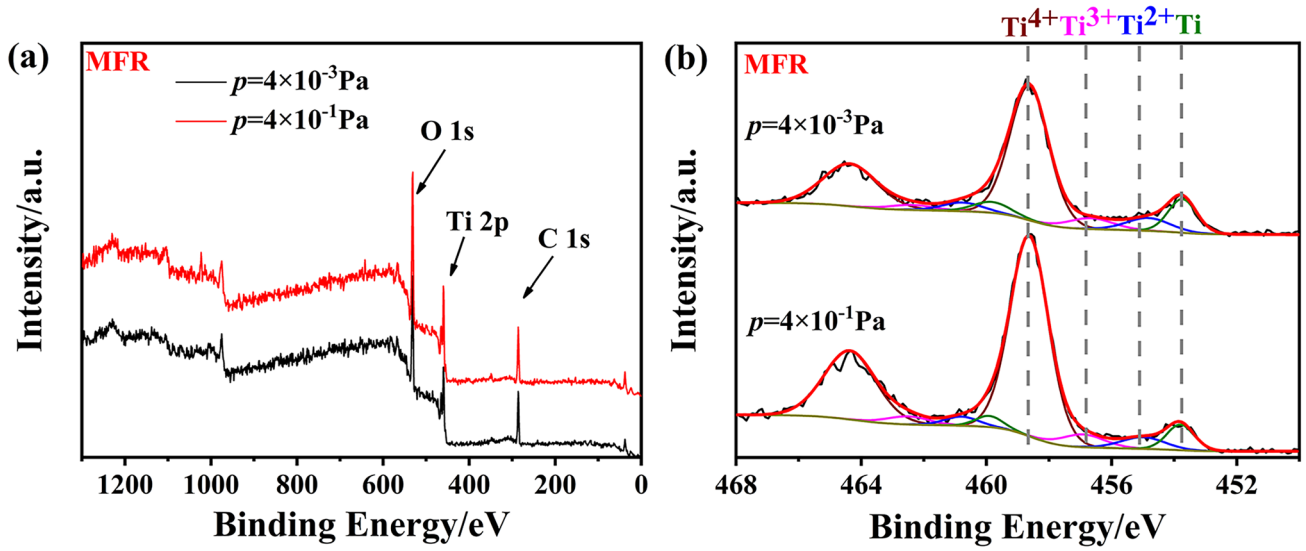

Fig. 5 XPS spectra of the worn scars in MFR. **a** the survey spectra. **b** Ti 2p ($D = 5$ μm)

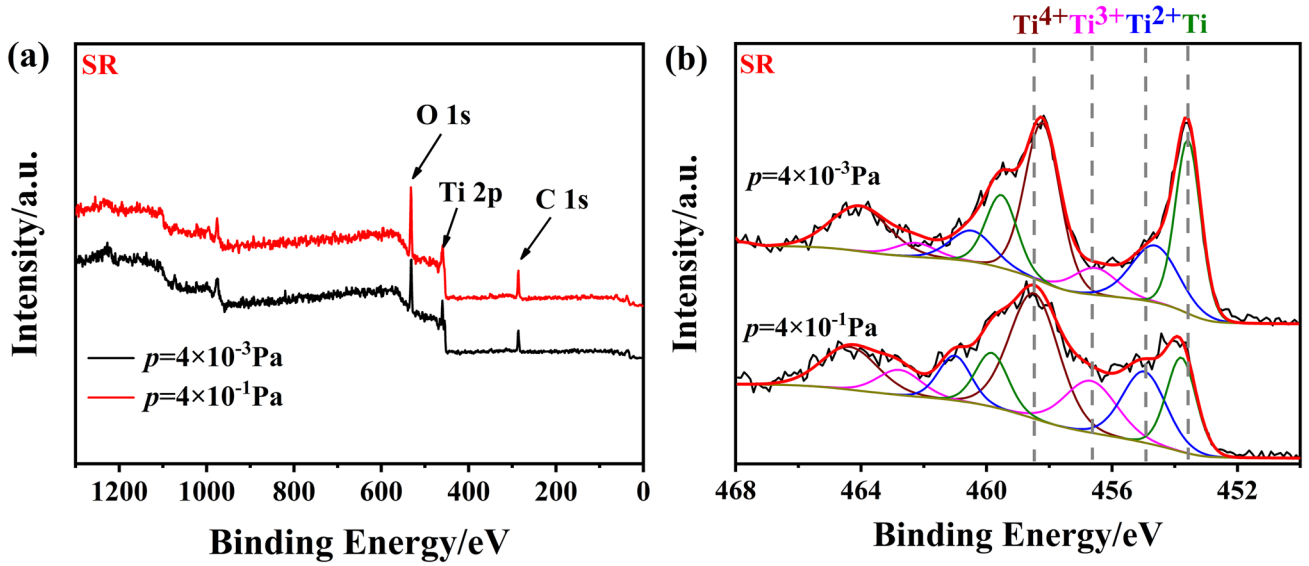

Fig. 6 XPS spectra of the worn scars in GSR. **a** the survey spectra. **b** Ti 2p ($D=30$ μm)

Table 3 Percentage contents of titanium oxides of worn scars under different conditions (at.%)

Test conditions	PSR ($D=1$ μm)				MFR ($D=5$ μm)				GSR ($D=30$ μm)			
Element	Ti^{4+}	Ti^{3+}	Ti^{2+}	Ti	Ti^{4+}	Ti^{3+}	Ti^{2+}	Ti	Ti^{4+}	Ti^{3+}	Ti^{2+}	Ti
$p=4\times10^{-1}$ Pa	0.84	0.07	0.03	0.06	0.81	0.06	0.06	0.07	0.40	0.18	0.21	0.21
$p=4\times10^{-3}$ Pa	0.81	0.07	0.07	0.05	0.72	0.06	0.09	0.13	0.40	0.08	0.20	0.32

vacuum degree there is a higher percentage of Ti_2O_3 and TiO, while under the high vacuum degree there is a higher percentage of Ti pure metal. During the fretting wear process, the oxidation and mechanical deformation are intrinsically coupled. The oxidation layer on the top surface can be crimped and broken under the mechanical deformation, and hence more fresh Ti metal was exposed yet meanwhile was suffered from the mixture of mechanical deformation and oxidation again. Under the high vacuum atmosphere, especial for the 4×10^{-3} Pa, the oxidation reaction was inhibited along with the mechanical mixing, hence showing more Ti metal on the worn scar.

The XPS results as discussed above clearly point out that the tribo-chemical state induced by fretting wear under varied specific atmospheres is significantly different depending on the fretting run regime, which hence could lead to remarkably different fretting wear behavior.

3.3 Damage Observations and Wear Mechanisms

After the fretting wear tests under the 4×10^{-3} Pa, 4×10^{-1} Pa, samples produced under 20N in different fretting running regimes, i.e., PSR ($D=1$ μm), MFR ($D=5$ μm) and GSR ($D=30$ μm) were selected for further morphological observations and wear mechanism analysis of worn surfaces.

3.3.1 Partial Slip Regime

Figure 7 displays the worn scar of Ti6Al4V titanium alloy in partial slip regime (PSR, $D=1$ μm) with the normal load of 20 N under the vacuum atmospheres. In the partial slip regime, due to much small displacement amplitude imposed, the reciprocating displacement was mainly the result of the elastic deformation of contact surface and the compliance of the tribo-system [32]. On the basis of the Mindlin's theory [33], a maximum value of Hertzian contact pressure is produced at the center of contact area and gradually decreases outwards. The distribution of the Hertz contact pressure will give rise to the stick at the center of contact surface and then the occurrence of micro-slip at the contact edge, consequently leading to the formation of wear annulus around the edge of the contact zone. As shown in Fig. 7, a typical worn scar morphology with a sticky contact zone at the center and wear annulus at the edge can be observed on the contact surface in PSR. Given the much small displacement hence almost no relative motion, the contact surfaces are often suffered from a very slight damage, as seen in Fig. 7 where the worn scars all look smooth. In contrast, for 4×10^{-1} Pa, there is no evident worn scar trace without clear wear annulus as seen in Fig. 7b, which is similar to that under the air atmosphere as reported in Refs. [21, 27]. As stated earlier, in PSR

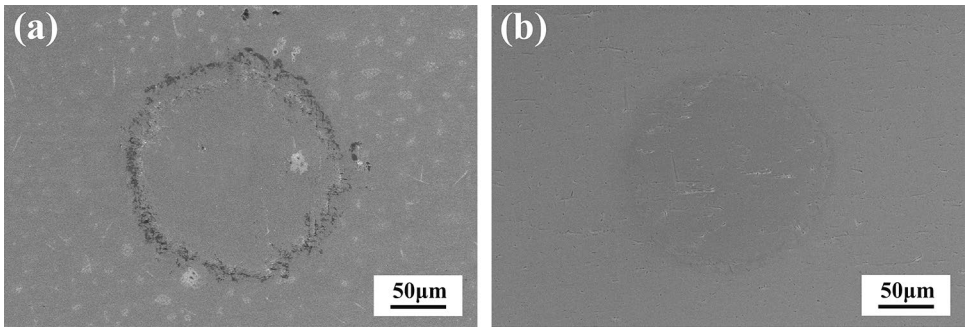

Fig. 7 SEM of worn scars of Ti6Al4V titanium alloy in PSR under **a** 4×10^{-3} Pa and **b** 4×10^{-1} Pa

the relative motion is mainly coordinated by elastic deformation. Given that the high degree of vacuum atmosphere can generally strengthen the adhesion of contact interface, under the high vacuum degree of 4×10^{-3} Pa the displacement motion could be mainly realized by micro-slip on the contact edge because of the stick at the center of contact surface as seen in Fig. 7a. While for the low vacuum degree of 4×10^{-1} Pa the relative motion may be coordinated by elastic deformation of the whole contact interface, hence leading to the worn scar morphology of Fig. 7b. In addition, combined with the XPS result of Fig. 4 which indicates that the contact interface is mainly TiO_2 originated from the initial surface of polished samples, the samples present very slight damage in PSR.

3.3.2 Mixed Fretting Regime

Figure 8 illustrates the damage mechanism of Ti6Al4V titanium alloy in mixed fretting regime (MFR, $D=5$ μm) under the normal load of 20 N under the vacuum atmospheres. It should be noted that the views presented in Fig. 8b, d are the resulting local magnified images of Fig. 8a, c as marked in red dash line, respectively. As can be seen in Fig. 8, the worn scars produced in two different vacuum atmospheres show different morphologies. In the case of 4×10^{-3} Pa (the high vacuum degree), the worn surface looks relatively smooth. However, there are a lot of small craters dispersed on the worn scar, which may be related to the adhesion of Ti metal material to the counter-body. As seen in Fig. 9a–e, the EDS results indicate that the worn scar of counter-body has some mount of Ti, Al and V element, showing materials transfer from the Ti metal surface. On the basis of the XPS results in Table 3, the tribo-chemical products on the worn scar in MFR under the high degree of vacuum atmosphere (4×10^{-3} Pa) is equivalent to that in PSR, which indicates that in MFR the tribo-oxidation is still difficult to take place on the worn surface due to no gas adsorption on the contact interface. As a result, it mainly shows the crater damage

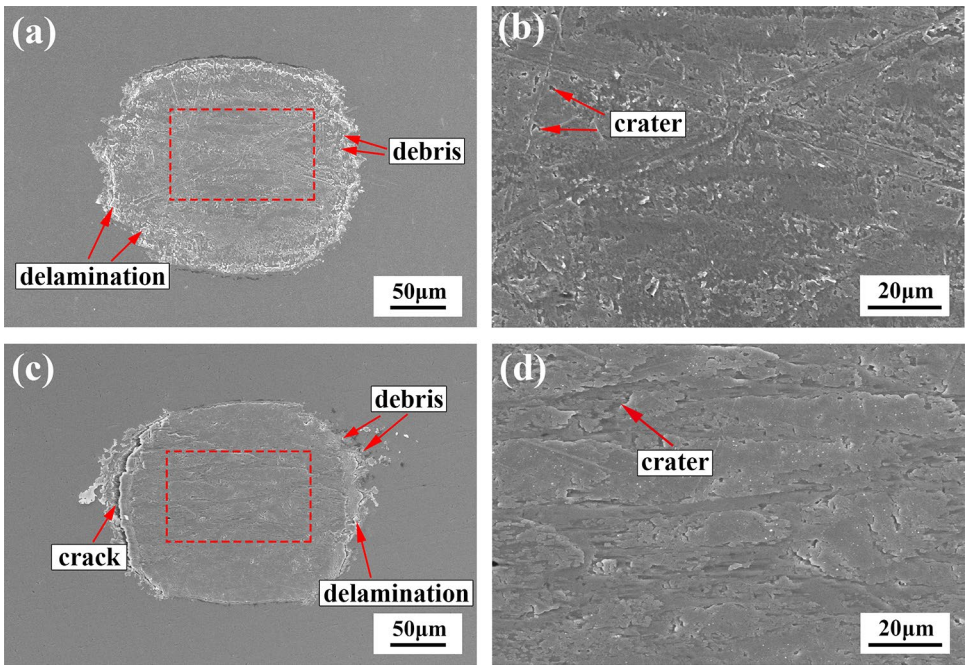

Fig. 8 SEM of worn scars of Ti6Al4V titanium alloy in MFR under **a** and **b** 4×10^{-3} Pa, **c** and **d** 4×10^{-1} Pa

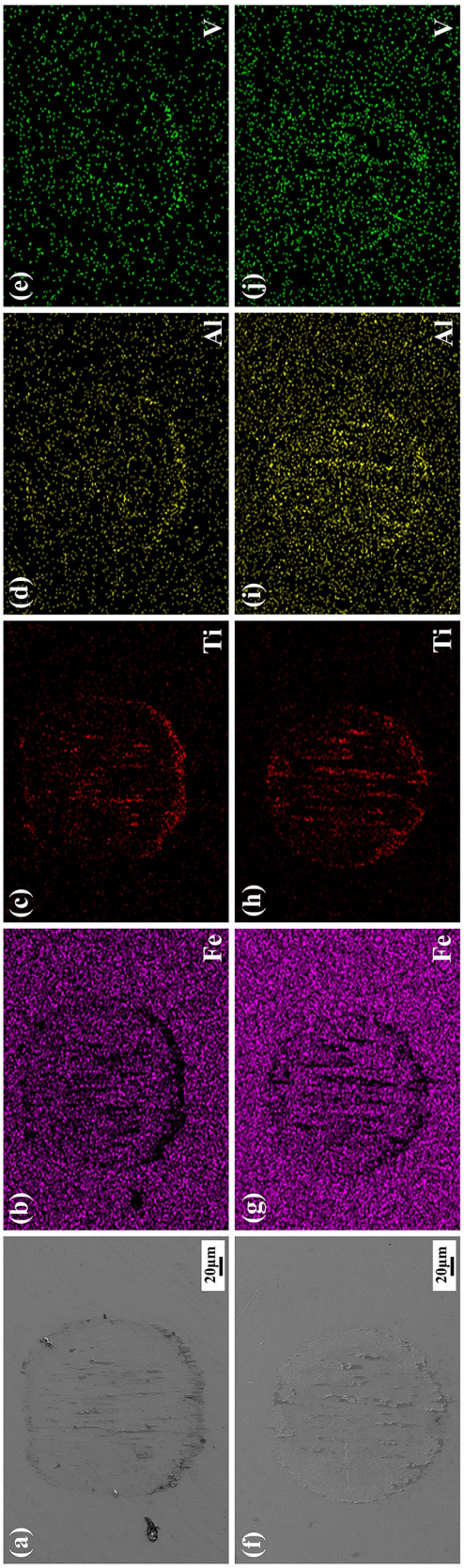

Fig. 9 SEM and EDS of worn scars of counter-body in MFR under **a–e** 4×10^{-3} Pa, **f–j** 4×10^{-1} Pa

due to the adhesion effect from micro-asperities shear under the tangential force as reported in Ref. [34]. While for the 4×10^{-1} Pa of low vacuum degree, the morphologies of the center worn surface of Ti metal and counter-body are similar to those created at 4×10^{-3} Pa atmosphere, which may be due to the possibility that the small displacement amplitude in MFR makes the center region of contact interface quasi-isolated from gas atmosphere, consequently leading to the result of equivalent atmosphere to 4×10^{-3} Pa atmosphere. The Ti metal material transfer to the counter-body can also be observed, as seen in Fig. 9f–j. On the edge of worn scar, however, the debris, delamination and cracks can be found as shown in Fig. 8c, which may be relevant to the possibility that the edge of worn scar was easily exposed to the as-received atmosphere and hence tribo-oxidation layer is relatively easier to be formed than that in the center of contact zone. Therefore, with the fretting wear process proceeds, tribo-oxidation film formed on the edge of worn scar was gradually sheared and subsequently broken in a plate-like shape, hence forming some delamination and debris as displayed in Fig. 8c. The morphology of worn scar produced in the 4×10^{-1} Pa suggests the main wear damage is adhesion wear accompanied by tribo-oxidation at the edge area.

3.3.3 Slip Regime

Figure 10 illustrates the damage mechanism of titanium alloy under the two different vacuum atmospheres in slip regime (GSR, $D=30$ μm). Similarly, the views presented in Fig. 10b, d are the local magnified images of Fig. 10a, c as marked in the red dash line, respectively. It is clear in GSR that the two different vacuum atmospheres cause significantly different morphologies of worn scars. Under the high vacuum condition (4×10^{-3} Pa), an evident plastic flow and adhesion shear can be observed and continuous wide furrows are distributed over the contact surface, as seen in Fig. 10a, b. The observations of cross section show a visible plastic deformation layer with a thin mechanical mixed layer (MML) on the top of surface, as seen in Fig. 11a. With the fretting wear process proceeds, the MML would be broken and formed discontinuous laminate-like flakes on the worn surface as seen in Fig. 10b. Upon the subsequent fretting wear events, the flakes were gradually grinded accompanied by delamination, to produce some debris and then micro-plough the worn surface. Meanwhile, the debris were gradually expelled from the contact zone during the reciprocating motions, finally accumulating around the outside edge of worn scar as seen in Fig. 10a. Moreover, as seen in Fig. 12a–e, a large amount of Ti metal material was transferred to the counter-body, presenting an evident adhesion effect taken placed on the contact interface. While for the low vacuum degree atmosphere of 4×10^{-1} Pa, the worn scar displays a

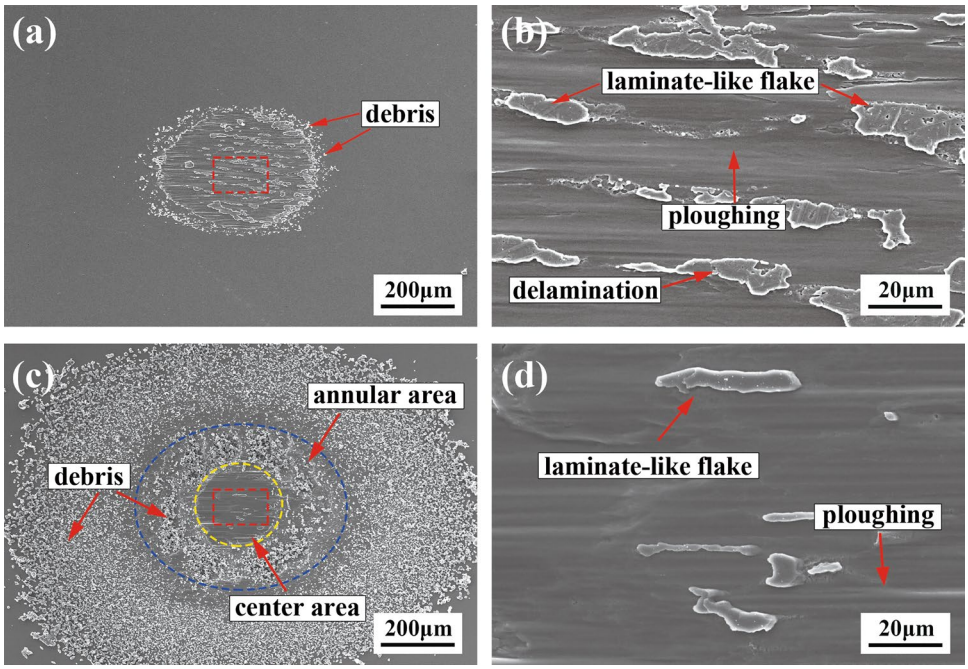

Fig. 10 SEM of worn scars of Ti6Al4V titanium alloy in GSR under **a** and **b** 4×10^{-3} Pa, **c** and **d** 4×10^{-1} Pa

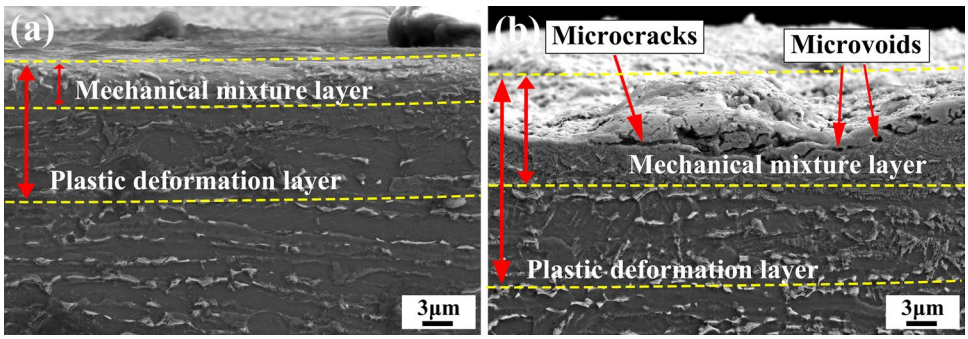

Fig. 11 The subsurface of worn scars in GSR for **a** 4×10^{-3} Pa, **b** 4×10^{-1} Pa

different serious damage morphology with lots of debris. It is interesting to notice that the contact zone seems to show two distinct zones like swimming ring (seen in Fig. 10c), i.e., (1) the center of the ring marked in the yellow dash line (the center of contact zone) which is very smooth accompanied by a few laminate-like flakes without much debris and (2) annular area between the blue dash line (the edge of worn scar distinguished by 3D profiles with the white light interferometer) and the yellow dash line which is covered with lots of small debris. Combined with the SEM images on the cross section (seen in Fig. 11b), there are much thicker MML within the plastic deformation layer as well, but it can be observed that the MML is uncompacted with lots of micro-cracks and micro-voids inside. As discussed above for the tribo-chemical products on the worn scar, under the low vacuum degree of 4×10^{-1} Pa, there is much higher content of Ti_2O_3 formed on the worn scar than that under the high vacuum degree of 4×10^{-3} Pa. It may be deduced that the uncompacted MML formed during the process of fretting wear was gradually grinded and meanwhile was prone to produce a tribo-oxidation layer containing more Ti_2O_3 products under such vacuum atmosphere (4×10^{-1} Pa). It is clear that tribo-oxidation layer on the top surface of MML is quite loosen with many micro-voids and micro-cracks (seen in Fig. 11b), which is susceptible to be broken and then delaminated due to the cyclic interaction of the fretting wear contact and hence form lots of debris, eventually approaching a dynamic equilibrium of tribo-oxidation layer development and removal. Upon subsequent reciprocating fretting process, the debris were mechanically expelled from the worn scar, and even adhered on the contact surface of counter-body (i.e., evident material transfer as seen in Fig. 12f–j to be transferred to the outside of worn scars, finally leading to lots of debris accumulated around the edge of worn scars. It demonstrates that the main wear mechanisms are micro-ploughing, micro-cracking and tribo-oxidation, accompanied with material transfer. The systematic analysis of

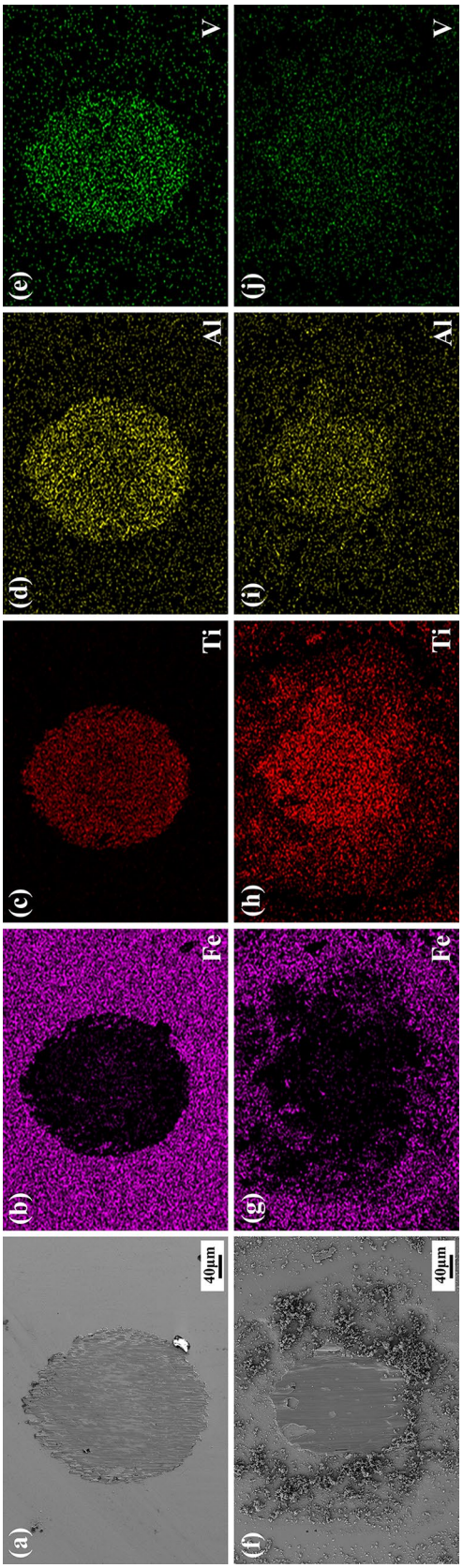

Fig. 12 SEM and EDS of worn scars of counter-body in GSR under **a–e** 4×10^{-3} Pa, **f–j** 4×10^{-1} Pa

worn scars reveals clearly the dependence of the damage mechanisms on fretting regime and the vacuum degree.

3.4 The Effect of Tribo-chemical State on the Fretting Wear

The results above reveal that the tribo-chemical state depends on not only the fretting regimes, but also the working atmosphere which can shift the damage mechanism from one type to another. In this section, of importance is to analyze the effect of tribo-chemical products on the friction coefficient and fretting wear resistance.

3.4.1 The Coefficient of Friction

The coefficient of friction (CoF) evolutions with cycles as taken in MFR under the two different vacuum degree conditions as an example is presented in Fig. 13a. Here, the CoF is defined as the ratio F_t^*/F_n, where F_n is the applied normal load, and the F_t^* is the average value of $F_{t,\max}$ and absolute value of ($-F_{t,\max}$) collected for each cycle, as stated in Ref. [25]. Furthermore, it is worth noting that, given that in PSR the reciprocating displacement was mainly coordinated by elastic deformation with almost no relative motion and hence the friction force is roughly equivalent to the static friction force, the ratio between tangential force and normal force (F_t^*/F_n) was defined as a nominal coefficient of friction in PSR. As can be seen in Fig. 13a, as the number of cycle approaches 2000 cycles around, the friction coefficient curve starts to keep stable, which demonstrates that the fretting wear commenced well to enter the steady state region within 2000 cycles after the onset of fretting wear. This implies that there are enough cycle numbers under which the fretting wear process is at a stable state. Figure 13b shows the average value of the stabilized coefficient of friction (CoF) of Ti6Al4V titanium alloy as a function of displacement amplitudes for the 4×10^{-3} Pa and 4×10^{-1} Pa conditions. It should also be noted that the determination of the stabilized coefficient of friction was referred to the Fouvry's work [35], i.e., the stable stage is corresponding to the [Nε, N] interval of cycle number among which the standard deviation of friction coefficient is less than 1.5%. Finally, a series of friction coefficients on the stable stage were averaged as the average value of the stabilized coefficient of friction. Although the evolutions of friction coefficient under two different vacuum atmospheres plotted in Fig. 13b see somewhat similar, in general they have different value of friction coefficient. It can be seen that the value of nominal friction coefficient in the PSR is quite low and equivalent. The low nominal friction coefficient in PSR could be attributed to the very small relative sliding, as well as the fact that the contact interface is mainly covered by TiO_2

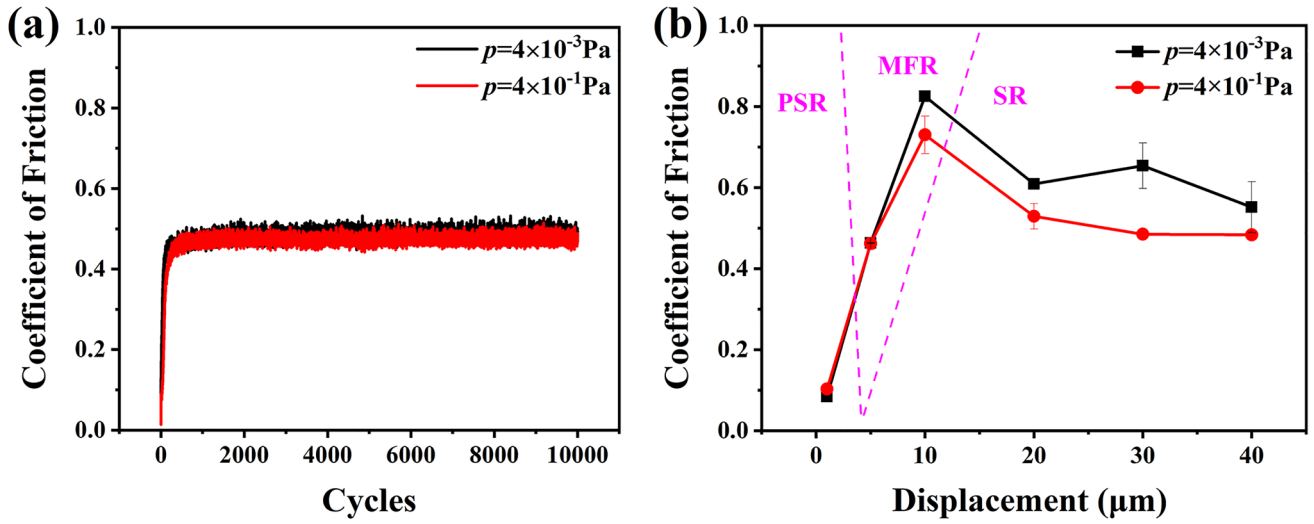

Fig. 13 **a** The evolution of coefficient of friction with the cycles under two different vacuum degree conditions ($D = 5$ μm), and **b** the average value of the stabilized coefficient of friction evolutions with the displacement amplitude under the two vacuum degree atmospheres

as seen in Fig. 4, which could provide lubrication role [36]. The equivalent nominal friction coefficient for the different vacuum degree may be due to the cause of nearly no relative sliding on the contact surface in PSR and the gas outside hardly enters into the contact interface zone, hence leading to equivalent situation of worn surface. Upon increasing the displacement amplitude to 5 μm, i.e., entering to the MFR, the relative motion of contact interface was coordinated by elastic–plastic deformation, and the content of TiO_2 gradually decreases but the Ti metal increase (seen in Table 3). As a consequent, both caused a rapid increase in friction coefficient as shown in Fig. 13b, which is consistent with the nature of adhesion in MFR [37]. Moreover, the increment of the friction coefficient for the 4×10^{-3} Pa (the high vacuum degree) is more noticeable than that for the 4×10^{-1} Pa, showing a higher value of 0.85 at the displacement amplitude of 10 μm. While with further increasing the displacement amplitude up to 20 μm, fretting wear all enter into the slip regime for all atmospheres. The friction coefficients under both vacuum atmospheres start to gradually decrease and then approach to a steady stage. Combined the XPS results and SEM images on the worn scars, in GSR there are lots of tribo-oxides debris formed, which could play a "third-body" role hence weaking the adhesion effect and decreasing the friction coefficient. Moreover, the samples under the two different vacuum degrees in GSR show different values in the friction coefficients, i.e., the sample under the low vacuum degree of 4×10^{-1} Pa has a lower friction coefficient than that under the high vacuum degree of 4×10^{-3} Pa, which could be attributed to the fact that the worn scars under the low vacuum degree of 4×10^{-1} Pa has lots of debris formed and plays a strong "third-body" effect hence reducing the friction coefficient, as stated in Ref. [38].

3.4.2 The Fretting Wear Resistance

As discussed above, the contact interface of a sample subjected to fretting wear in the different specific vacuum environment will create different tribo-chemical state, which consequently plays a significant effect on the fretting friction coefficient, damage mechanism, and hence fretting wear resistance. Figures 14 and 15 show the fretting wear volume of worn scar and the two-dimensional profiles perpendicular to the sliding direction at the center of worn scars for different fretting run regimes under the different vacuum environments, respectively. In addition, in order to benchmark the fretting wear volume under the vacuum atmospheres, the fretting wear volume under the air atmosphere as reported in previous work [27] as well as the resulting profiles of worn scars were also plotted in Figs. 14 and 15, respectively. It should be noted that the calculated fretting wear volume is the volume loss below the baseline of the original surface of samples without involving the pile-ups. Prior to the measurement of wear loss, the sample after wear test was ultrasonically cleaned, mainly aiming to remove the debris and pollutions attached on the worn scars. It is also worth pointing out that, the pile-ups were the main result of the plastic deformation, which was hardly removed by the ultrasonic cleaning and is marginal compared to the measured wear volume in the current paper (as shown in the 2D profiles of the center of the worn scars in Fig. 15). Therefore, the volume loss below the baseline of the original surface of

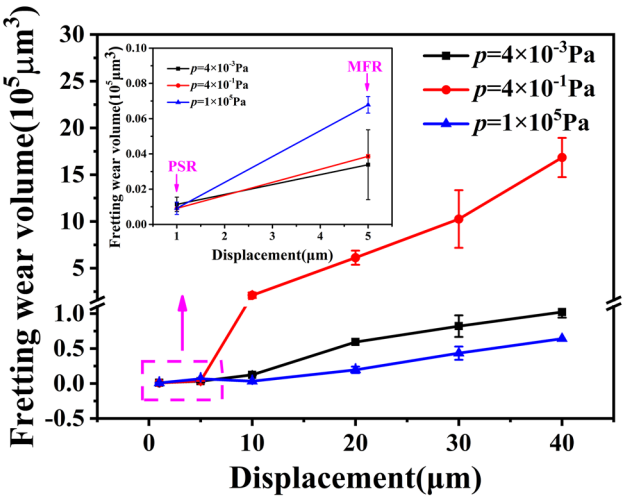

Fig. 14 The fretting wear volume evolutions of Ti6Al4V titanium alloy with the displacement amplitude in the different fretting regimes under different atmospheres (Note: the data points on wear volume in the 1×10^5 Pa was reported in Ref. [27]. and three data points on wear volume in the 4×10^{-3} Pa was reported in Ref. [45].)

samples was used as a parameter to rank the fretting wear resistance. It is clear that, as the displacement amplitude is less than 5 μm, i.e., in the PSR, the samples have comparable fretting wear volume with a very low value (seen in the inset of Fig. 14) despite of the different testing atmosphere, which is well consistent with the results of the worn scar profiles as seen in Fig. 15. The wear damage is in good agreement with the XPS results in PSR (shown in Fig. 4) in which the tribo-chemical states of worn surfaces subjected to the different atmospheres are equivalent, i.e., mainly composed of TiO_2 oxide film. According to the statement above, the dominant TiO_2 should be originated from the initial surface of polished sample, which implies a very mild damage hence leading to a very low fretting wear volume.

While for the MFR, the fretting wear volume of worn scars generally decreases with the increase of vacuum degree. As discussed above, with increasing the vacuum degree, there are less TiO_2 oxides formed and hence more Ti metal exposed on the contact surface (seen in Table 3). It will enhance the adhesion effect of contact interface and hence show a higher friction coefficient as shown in Fig. 13. Given that in MFR the displacement amplitude is still small and mainly complies with elastic–plastic deformation, the enhancement of adhesion effect will decrease the relative motion of contact interface, hence reducing the fretting wear damage. It can also be seen in Fig. 15b that the samples in the vacuum atmospheres have shallower worn scar profile than that in the air atmosphere. In addition, the sample under the vacuum atmosphere seems to present a compacted worn surface, which can play an effective protection role as stated by Wang [13]. As a consequence, in MFR there is a milder damage at a higher vacuum degree, and hence the damage under the air atmosphere is the most serious.

As entering the GSR, the fretting wear volumes of samples all increase fast with the increase of displacement amplitude. It is interesting to note that the increase in fretting wear volume for the low vacuum degree (4×10^{-1} Pa) is most noticeable, showing a highest fretting wear volume and hence a largest depth and width of worn scar (seen in Fig. 15c), which is consistent with the SEM images of worn scars in Fig. 10. In contrast, the fretting wear volume for the air atmosphere (1×10^5 Pa) is lowest. The order of fretting wear volume follows 1×10^5 Pa, 4×10^{-3} Pa and 4×10^{-1} Pa, which is in line with the results as shown in Fig. 15c. Based on the XPS results of Fig. 6, in the case of the vacuum atmosphere, there are less content of TiO_2 (40%) but more Ti, TiO and Ti_2O_3 produced on the worn surface in GSR. It indicates that the Ti metal seems to be prone to be oxidized to Ti_2O_3 and TiO, especially for the low vacuum degree (4×10^{-1} Pa) showing a highest percentage of Ti_2O_3 (18%). As discussed above, for the 4×10^{-1} Pa condition, it might be inferred that the tribo-oxidation layer containing more Ti_2O_3 products on the top surface of MML seems to be susceptible to be broken, consequently forming lots of debris on the worn scar, wich is consistent with the previous study in Ref. [27]. In general, the debris is considered as the third body, which can separate the contacting bodies, carry the load and delay the further deterioration on worn surface [39]. Actually, however, the role of the debris is determined by the trad-off between the rate of debris formation within the contact interface (rate of oxygen input) and the rate of debris ejection from the contact interface [40, 41]. Accordingly, given that the debris formed under 4×10^{-1} Pa condition were small and loosened (seen in Fig. 10c), they seem to be easy to be ejected from the worn scar upon subsequent reciprocating fretting process, hence providing a marginal protection against fretting wear and even aggravating wear damage by ploughing upon the brittle debris as stated in Ref. [12, 42]. As a result, it shows a highest fretting wear volume under 4×10^{-1} Pa condition. While for the air environment [27], the worn surface was mainly covered by compacted MML containing TiO_2 (nearly without Ti_2O_3 and TiO), which could give a good protection against fretting wear [13, 43, 44]. Compared to the air atmosphere, therefore, Ti6Al4V under the vacuum atmosphere presents a higher fretting wear volume in GSR. The results may also suggest that for the vacuum environments, the Ti6Al4V is more suitable to be used under the high vacuum atmosphere in GSR under which it could inhabit the formation of Ti_2O_3. Moreover, the results above may can be applied to identify the optimal vacuum condition of Ti6Al4V and hence to tune the application environment condition or provide the guideline

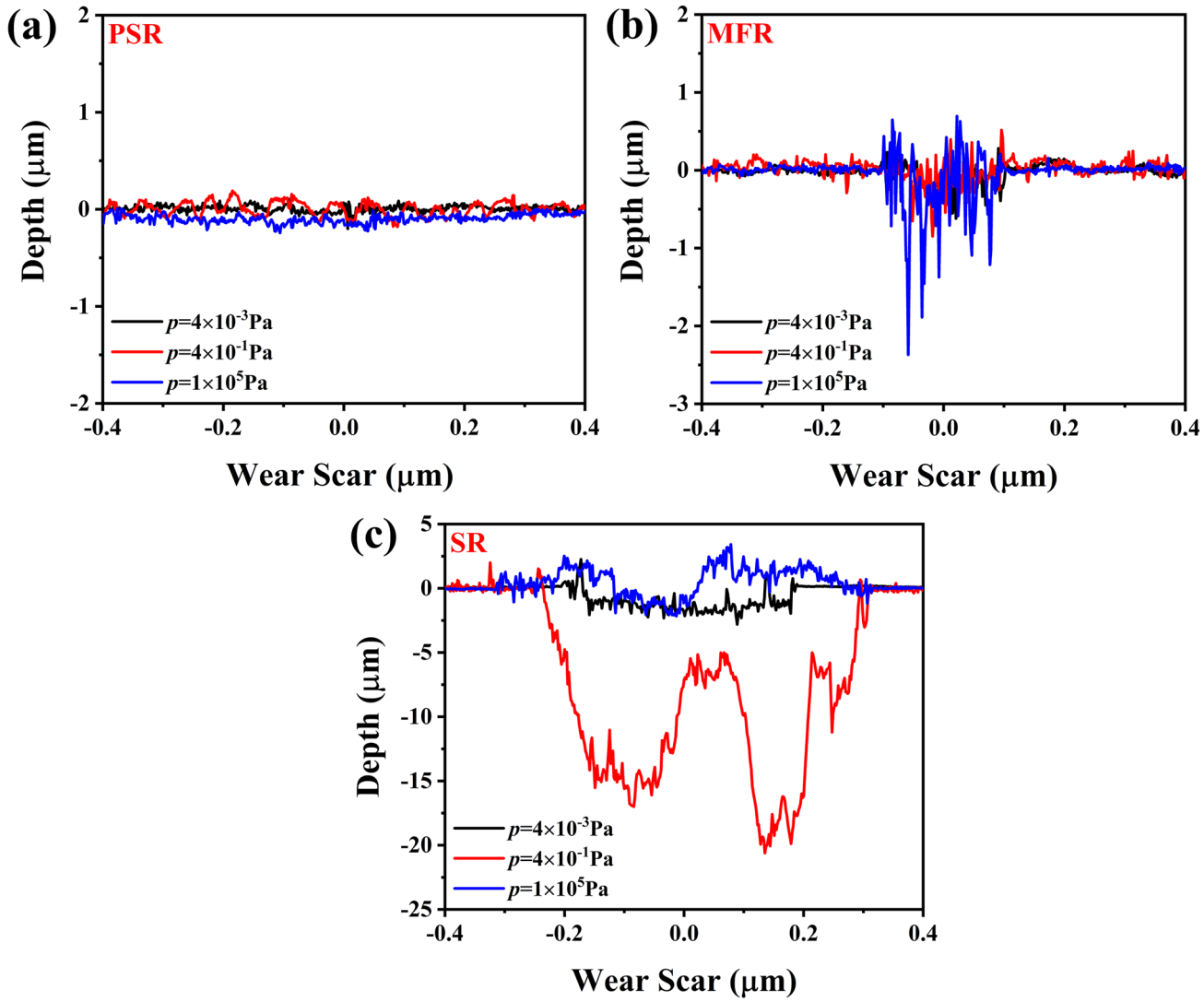

Fig. 15 Two-dimensional profiles of the worn scars of Ti6Al4V titanium alloy under different atmospheres in the different fretting regimes: **a** PSR, **b** MFR, and **c** GSR

to select the proper fretting regimes by tribological design so as to optimize the performance of the titanium components.

4 Conclusions

In the present work, an in situ XPS analysis tester was developed by a self-designed high precision fretting wear tester integrated with an X-ray photoelectron spectroscopy (XPS) equipment, aiming to probe the tribo-chemical state of worn surface of Ti6Al4V titanium alloy under the vacuum atmospheres and study its correlation with the resulting damage mechanism and fretting wear resistance. On the basis of the experimental observations and tribo-chemical state analysis, the following conclusions can be draw:

(1) The tribo-chemical state of worn scars produced during fretting wear process under vacuum atmosphere is strongly dependent on the fretting regimes, which plays a significantly different role in determining the wear damage and hence fretting wear resistance.
(2) In PSR, the worn scars were mainly covered by TiO_2 under both vacuum atmospheres, which were dominantly originated from the initial surface of polished sample, showing comparable levels of very mild damage. In MFR, besides an evident exposure of Ti metal for the high vacuum degree (4×10^{-3} Pa), the tribo-layers are still mainly consisted of TiO_2 under both vacuum atmospheres, showing dominant adhesive wear, along with the delamination on the edge of worn scars in the low vacuum degree (4×10^{-3} Pa).

(3) In GSR, the tribo-chemical products of worn scars are consisted of TiO_2, TiO and Ti_2O_3, Ti metal, which indicates that Ti metal was prone to be oxidized to Ti_2O_3 and TiO under the vacuum atmospheres, especially for the low vacuum degree (4×10^{-1} Pa) having a highest content of Ti_2O_3. It might be inferred that the tribolayer containing more Ti_2O_3 may seem to be susceptible to be broken during fretting wear process, hence leading to a highest fretting wear volume in the low vacuum degree atmosphere (4×10^{-1} Pa).

(4) Compared to the air atmosphere, the sample in the vacuum has a comparable level of fretting wear resistance in PSR, and better fretting wear resistance in MFR, but lower fretting wear resistance in GSR.

(5) The results above may also can be applied to identify the optimal vacuum condition of Ti6Al4V and hence to tune the application environment condition or provide the guideline to select the proper fretting regimes by tribological design so as to allow a best performance of the titanium component.

Acknowledgements The authors gratefully acknowledge financial support provided by Sichuan Science and Technology Program (2023NSFSC0413), the Natural Science Foundation of China (51575459) and the Fundamental Research Funds for the Central Universities (2682023GF018).

Author Contributions Jianjun Long and Xuejiao Wei: experiments, data analysis and manuscript preparation. Xixi Cheng, Yiting Dong and Hao Li: materials characterization and data analysis. Xiaojun Xu and Minhao Zhu: supervision, funding acquisition and the revision and embellishment of the manuscript.

Funding This work was supported by the Sichuan Science and Technology Program (2023NSFSC0413), the Natural Science Foundation of China (51575459) and the Fundamental Research Funds for the Central Universities (2682023GF018).

Data Availability The data used in this research are available upon request. Please contact the corresponding author for access to the data.

Declarations

Competing interests The authors declare no competing interests.

References

1. Lee, Y.H., Kim, H.K.: Fretting wear behavior of a nuclear fuel rod under a simulated primary coolant condition. Wear **301**, 569–574 (2013). https://doi.org/10.1016/j.wear.2013.01.067
2. Liu, H.W., Xu, X.J., Zhu, M.H., Ren, P.D., Zhou, Z.R.: High temperature fretting wear behavior of WC–25Co coatings prepared by D-gun spraying on Ti–Al–Zr titanium alloy. Tribol. Int. **44**, 1461–1470 (2011). https://doi.org/10.1016/j.triboint.2011.01.002
3. Shen, Y., Zhang, D., Ge, S.: Effect of fretting amplitudes on fretting wear behavior of steel wires in coal mines. Min. Sci. Technol. **20**, 803–808 (2010). https://doi.org/10.1016/S1674-5264(09)60285-4
4. Yang, Y., Wang, C., Gesang, Y., Shang, H., Wang, R., Liang, Y., Wang, T., Chen, Q., Shao, T.: Fretting wear evolution of γ-TiAl alloy. Tribol. Int. **154**, 106721 (2021). https://doi.org/10.1016/j.triboint.2020.106721
5. Dong, H., Bell, T.: Tribological behaviour of alumina sliding against Ti6Al4V in unlubricated contact. Wear **225–229**, 874–884 (1999). https://doi.org/10.1016/S0043-1648(98)00407-4
6. Lebedeva, I.L., Presnyakova, G.N.: Adhesion wear mechanisms under dry friction of titanium alloys in vacuum. Wear **148**, 203–210 (1991). https://doi.org/10.1016/0043-1648(91)90284-2
7. Diomidis, N., Mischler, S.: Third body effects on friction and wear during fretting of steel contacts. Tribol. Int. **44**, 1452–1460 (2011). https://doi.org/10.1016/j.triboint.2011.02.013
8. Mary, C., Le Mogne, T., Beaugiraud, B., Vacher, B., Martin, J.M., Fouvry, S.: Tribochemistry of a Ti alloy under fretting in air: evidence of titanium nitride formation. Tribol. Lett. **34**, 211–222 (2009). https://doi.org/10.1007/s11249-009-9426-6
9. Wit, Ed., Blanpain, B., Froyen, L., Celis, J.P.: The tribochemical behaviour of TiN-coatings during fretting wear. Wear **217**, 215–224 (1998). https://doi.org/10.1016/S0043-1648(98)00183-5
10. Molinari, A., Straffelini, G., Tesi, B., Bacci, T.: Dry sliding wear mechanisms of the Ti6Al4V alloy. Wear **208**, 105–112 (1997). https://doi.org/10.1016/S0043-1648(96)07454-6
11. Farokhzadeh, K., Edrisy, A.: Transition between mild and severe wear in titanium alloys. Tribol. Int. **94**, 98–111 (2016). https://doi.org/10.1016/j.triboint.2015.08.020
12. Li, X.X., Zhou, Y., Li, Y.X., Ji, X.L., Wang, S.Q.: Dry sliding wear characteristics of Ti-6.5Al-3.5Mo-1.5Zr-0.3Si alloy at various sliding speeds. Metall. Mater. Trans. A **46**, 4360–4368 (2015). https://doi.org/10.1007/s11661-015-3019-9
13. Wang, L., Zhang, Q.Y., Li, X.X., Cui, X.H., Wang, S.Q.: Severe-to-mild wear transition of titanium alloys as a function of temperature. Tribol. Lett. **53**, 511–520 (2014). https://doi.org/10.1007/s11249-013-0289-5
14. Wang, L., Zhang, Q.Y., Li, X.X., Cui, X.H., Wang, S.Q.: Dry Sliding Wear Behavior of Ti-6.5Al-3.5Mo-1.5Zr-0.3Si Alloy. Metall. Mater. Trans. A **45**, 2284–2296 (2014). https://doi.org/10.1007/s11661-013-2167-z
15. Hierro-Oliva, M., Gallardo-Moreno, A.M., González-Martín, M.L.: XPS analysis of Ti6Al4V oxidation under UHV conditions. Metall. Mater. Trans. A **45**, 6285–6290 (2014). https://doi.org/10.1007/s11661-014-2570-0
16. Alam, M.O., Haseeb, A.S.M.A.: Response of Ti–6Al–4V and Ti–24Al–11Nb alloys to dry sliding wear against hardened steel. Tribol. Int. **35**, 357–362 (2002). https://doi.org/10.1016/S0301-679X(02)00015-4
17. Mao, Y.S., Wang, L., Chen, K.M., Wang, S.Q., Cui, X.H.: Tribolayer and its role in dry sliding wear of Ti–6Al–4V alloy. Wear **297**, 1032–1039 (2013). https://doi.org/10.1016/j.wear.2012.11.063
18. Mercer, A.P., Hutchings, I.M.: The influence of atmospheric composition on the abrasive wear of titanium and Ti-6Al-4V. Wear **124**, 165–176 (1988). https://doi.org/10.1016/0043-1648(88)90242-6
19. Liu, Y., Yang, D.Z., He, S.Y., Wu, W.L.: Microstructure developed in the surface layer of Ti-6Al-4V alloy after sliding wear in vacuum. Mater. Charact. **50**, 275–279 (2003). https://doi.org/10.1016/s1044-5803(03)00125-6
20. Yang, L.Q., Zhong, H., Lv, G., Yue, Y., Guo, B.Y., Ma, M.Z., Liu, R.P.: Dry sliding behavior of a TiZr-based alloy under air and vacuum conditions. J. Mater. Eng. Perform. **28**, 3402–3412 (2019). https://doi.org/10.1007/s11665-019-04100-4
21. Chelliah, N., Kailas, S.V.: Synergy between tribo-oxidation and strain rate response on governing the dry sliding wear behavior

of titanium. Wear **266**, 704–712 (2009). https://doi.org/10.1016/j.wear.2008.08.011
22. Zhong, H., Dai, L.Y., Yang, Y.J., Yue, Y., Wang, B.A., Zhang, X.Y., Ma, M.Z., Liu, R.P.: Vacuum tribological properties of Ti-20Zr-6.5Al-4V alloy as influenced by sliding velocities. Metall. Mater. Trans. A **48**, 5678–5687 (2017). https://doi.org/10.1007/s11661-017-4301-9
23. Yazdanian, M.M., Edrisy, A., Alpas, A.T.: Vacuum sliding behaviour of thermally oxidized Ti–6Al–4V alloy. Surf. Coat. Technol. **202**, 1182–1188 (2007). https://doi.org/10.1016/j.surfcoat.2007.05.069
24. Zhou, Y., Shen, M., Cai, Z., Peng, J., Zhu, M.: Study on dual rotary fretting wear behavior of Ti6Al4V titanium alloy. Wear **376–377**, 670–679 (2017). https://doi.org/10.1016/j.wear.2016.10.027
25. Qiu, X., Wei, X., Xu, X., Xu, W., Zhu, M.: Dependence of fretting wear resistance on microstructural features of alloyed steels. Tribol. Int. **137**, 39–45 (2019). https://doi.org/10.1016/j.triboint.2019.04.028
26. Wei, X., Sheng, L., Li, H., Xu, X., Peng, J., Gou, G., Zhu, M.: The effect of oxygen pressure on the fretting wear of titanium alloys. Int. J. Mod. Phys. B **34**, 2050128 (2020). https://doi.org/10.1142/s0217979220501283
27. Cheng, X., Wei, X., Li, H., Wei, H., Xu, X., Sheng, L., Zhu, M.: Investigation on the fretting wear behavior of titanium alloy under different atmospheres by an in situ XPS spectrometry. Int. J. Mod. Phys. B **36**, 2250109 (2022). https://doi.org/10.1142/s0217979222501090
28. Zhou, Z.R., Nakazawa, K., Zhu, M.H., Maruyama, N., Kapsa, P., Vincent, L.: Progress in fretting maps. Tribol. Int. **39**, 1068–1073 (2006). https://doi.org/10.1016/j.triboint.2006.02.001
29. Zhu, M.H., Zhou, Z.R.: On the mechanisms of various fretting wear modes. Tribol. Int. **44**, 1378–1388 (2011). https://doi.org/10.1016/j.triboint.2011.02.010
30. Fouvry, S., Kapsa, P., Vincent, L.: Analysis of sliding behaviour for fretting loadings: determination of transition criteria. Wear **185**, 35–46 (1995). https://doi.org/10.1016/0043-1648(94)06582-9
31. Chaudhry, V., Kailas, S.V.: Damage mechanisms in stainless steel and chromium carbide coatings under controlled environment fretting conditions. Wear **334–335**, 75–81 (2015). https://doi.org/10.1016/j.wear.2015.01.001
32. Vingsbo, O., Söderberg, S.: On fretting maps. Wear **126**, 131–147 (1988). https://doi.org/10.1016/0043-1648(88)90134-2
33. Mindlin, R.D.: Compliance of elastic bodies in contact. J. Appl. Mech. **16**, 529–268 (1949). https://doi.org/10.1115/1.4009973
34. Dearnley, P.A., Dahm, K.L., Çimenoğlu, H.: The corrosion–wear behaviour of thermally oxidised CP-Ti and Ti–6Al–4V. Wear **256**, 469–479 (2004). https://doi.org/10.1016/s0043-1648(03)00557-x
35. Mary, C., Fouvry, S., Martin, J.M., Bonnet, B.: High temperature fretting wear of a Ti alloy/CuNiIn contact. Surf. Coat. Technol. **203**, 691–698 (2008). https://doi.org/10.1016/j.surfcoat.2008.08.043
36. Gu, Y., Zhao, X., Liu, Y., Lv, Y.: Preparation and tribological properties of dual-coated TiO2 nanoparticles as water-based lubricant additives. J. Nanomater. **2014**, 1–8 (2014). https://doi.org/10.1155/2014/785680
37. Zhou, Z.R., Vincent, L.: Mixed fretting regime. Wear **181–183**, 531–536 (1995). https://doi.org/10.1016/0043-1648(95)90168-X
38. Zhang, Y., Mollon, G., Descartes, S.: Significance of third body rheology in friction at a dry sliding interface observed by a multi-body meshfree model: Influence of cohesion between particles. Tribol. Int. **145**, 106188 (2020). https://doi.org/10.1016/j.triboint.2020.106188
39. Godet, M.: The third-body approach: a mechanical view of wear. Wear **100**, 437–452 (1984). https://doi.org/10.1016/0043-1648(84)90025-5
40. Kirk, A.M., Sun, W., Bennett, C.J., Shipway, P.H.: Interaction of displacement amplitude and frequency effects in fretting wear of a high strength steel: Impact on debris bed formation and subsurface damage. Wear **482–483**, 203981 (2021). https://doi.org/10.1016/j.wear.2021.203981
41. Zhu, T., Shipway, P.H., Sun, W.: The dependence of wear rate on wear scar size in fretting; the role of debris (third body) expulsion from the contact. Wear **440–441**, 203081 (2019). https://doi.org/10.1016/j.wear.2019.203081
42. Ming, Q., Yongzhen, Z., Jun, Z., Jianheng, Y.: Correlation between the characteristics of the thermo-mechanical mixed layer and wear behaviour of Ti–6Al–4V alloy. Tribol. Lett. **22**, 227–231 (2006). https://doi.org/10.1007/s11249-006-9088-6
43. Singh, K., Raman, S.G.S., Gnanamoorthy, R.: Effect of thermal oxidation duration on fretting wear behavior of Ti6Al4V in Ringer's solution. Trans. Indian Inst. Met. **75**, 1629–1639 (2022). https://doi.org/10.1007/s12666-022-02543-3
44. Wang, S., Liao, Z., Liu, Y., Liu, W.: Influence of thermal oxidation duration on the microstructure and fretting wear behavior of Ti6Al4V alloy. Mater. Chem. Phys. **159**, 139–151 (2015). https://doi.org/10.1016/j.matchemphys.2015.03.063
45. Sheng, L., Deng, X., Li, H., Ren, Y., Gou, G., Xu, X., Wang, Z., Zhu, M.: Fretting wear behavior of thermal-oxidation on titanium alloy in air and vacuum atmosphere. Int. J. Mod. Phys. B **35**, 2150135 (2021). https://doi.org/10.1142/s0217979221501356